Stem Cell Research & Therapy

RESEARCH

Open Access

MSCs-derived HGF alleviates senescence by inhibiting unopposed mitochondrial fusion-based elongation in post-acute kidney injury

Kaiting Zhuang[1,2], Wenjuan Wang[2], Xumin Zheng[1,2], Xinru Guo[3], Cheng Xu[2], Xuejing Ren[2], Wanjun Shen[2], Qiuxia Han[4], Zhe Feng[2], Xiangmei Chen[2] and Guangyan Cai[2*]

Abstract

Background The underlying mechanism of human umbilical-derived mesenchymal stem cells (hUC-MSCs) therapy for renal senescence in post-acute kidney injury (post-AKI) remains unclear. Unopposed mitochondrial fusion-based mitochondrial elongation is required for cellular senescence. This study attempted to dissect the role of hUC-MSCs therapy in modulating mitochondrial elongation-related senescence by hUC-MSCs therapy in post-AKI.

Methods Initially, a unilateral renal ischemia–reperfusion (uIRI) model was established in C57 mice. Subsequently, lentivirus-transfected hUC-MSCs were given by subcapsular injection. Two weeks after transplantation, histochemical staining, and transmission electron microscopy were used to assess the efficacy of hUC-MSCs in treating renal senescence, fibrosis, and mitochondrial function. To further investigate the mitochondrial regulation of hUC-MSCs secretion, hypoxic HK-2 cells were built. Finally, antibodies of HGF and its receptor were used within the hUC-MSCs supernatant.

Results Unopposed mitochondrial fusion, renal senescence, and renal interstitial fibrosis were successively identified after uIRI in mice. Then, the efficacy of hUC-MSCs after uIRI was confirmed. Subsequently, inhibiting hUC-MSCs-derived HGF significantly compromises the efficacy of hUC-MSCs and leads to ineffectively curbing mitochondrial elongation, accompanying insufficient control of elevated PKA and inhibitory phosphorylation of drp1 (Drp1pSer637). As a result, the treatment efficacy of renal senescence and fibrosis alleviation was also weakened. Furthermore, similar results were obtained with antibodies blocking HGF or cMet in hypoxic HK-2 cells treated with hUC-MSCs-condition medium for further proving. Uncurbed mitochondrial elongation induced by PKA and Drp1pSer637 was inhibited by hUC-MSCs derived HGF but reversed in the activation or overexpression of PKA.

Conclusions The research concluded that hUC-MSCs-derived HGF can inhibit PKA-Drp1pSer637-mitochondrial elongation via its receptor cMet to alleviate renal senescence and fibrosis in post-AKI.

Keywords Renal premature senescence, Mesenchymal stem cells (MSCs), Hepatocyte growth factor (HGF), Mitochondrial elongation

*Correspondence:
Guangyan Cai
caiguangyan@sina.com
Full list of author information is available at the end of the article

Introduction

Acute kidney injury (AKI), characterized by a sharp drop in glomerular filtration capacity, is a life-threatening clinical syndrome. Its mortality in intensive care units can be as high as 50% [1]. Post-acute kidney injury (post-AKI) is a condition with a persistent decline in renal function immediately following AKI. Abnormal cellular responses, epigenetic changes, and sustained proinflammatory signaling, especially cell-cycle arrest-driven cellular senescence in post-AKI, accelerate the onset of renal fibrosis [2]. Unfortunately, despite significant advances in our pathophysiological understanding, therapeutic options to prevent progressive fibrosis in post-AKI remain limited.

Recent studies have found that various types of AKI were followed by cellular senescence [3, 4]. Cellular senescence is a highly complex and finely regulated irreversible life event and thus become a research hotspot in recent years [5]. The underlying molecular mechanisms of cellular senescence include cell cycle arrest, oxidative stress, and DNA damage caused by post-AKI. Notably, Mitochondrial dysfunction has been found to play a crucial role in the development of post-AKI [6] and cellular senescence [7]. Dynamics-based mitochondrial dysfunction could result in renal senescence due to innate immune response activation, impaired redox regulation, imbalanced AMP/ATP ratios, or persistent DNA damage response [7]. Therefore, imbalanced dynamics can significantly contribute to stress-induced premature renal tubular epithelial senescence [6]. With well-planned molecular mechanisms, mitochondrial dynamics maintain morphological diversity by coordinating the repeated exchange of substances in space. Elongated and punctate mitochondria balance is essential for the mitochondrial dynamics network. Excessive mitochondrial elongation, a type of dynamics disturbance, is required for cellular senescence [8]. Possible triggers include hyperpolarization of the inner mitochondrial membrane, impaired aerobic respiration, changes in glycolytic and gluconeogenesis capacity, and disruptive fatty acid oxidation [9]. However, the extent to which mitochondrial elongation affects kidney disease remains unknown.

Various therapeutic techniques, especially mesenchymal stem cells (MSCs), are being explored to target cellular senescence, which could alleviate renal injury and protect renal function [10, 11]. Stem cell-based therapy has tremendous potential due to its ability to control mitochondrial dynamics, closely tied to pleiotropy. Recent studies have shown that MSCs can inhibit mitochondrial excessive fission [12] or promote fission-based mitochondrial biogenesis through deacetylase [13], which helps prevent pathological damage from post-AKI. Therefore, mitochondrial dynamic control under MSCs therapy is presented in a complex network rather than a single line. Excessive mitochondrial elongation, a flexible morphological transition that has been historically overlooked, might explain the aforementioned "paradox". However, the modulation of mitochondrial length overload by MSCs has yet to be fully explored. Recent research has shown that human umbilical cord-derived MSCs (hUC-MSCs) secrete hepatocyte growth factor (HGF), effectively treating elderly mitochondrial disease including Alzheimer's disease [14] and sarcopenia [15]. Additionally, the content of HGF in hUC-MSCs secretion was in the top three [14]. These findings prompted us to consider HGF as an anti-senescence and mitochondrial regulator in hUC-MSCs.

In the present study, to investigate the role of hUC-MSCs-derived HGF in renal senescence in post-AKI, viral transfection or antibody neutralization was utilized to inhibit hUC-MSCs-derived HGF. Furthermore, enzyme activity or gene expression manipulation was employed to uncover the downstream regulation of HGF.

Materials and method

Animal model and treatment

The work has been reported in line with the ARRIVE guidelines 2.0. Eight-week-old male C57BL/6 mice of uniform weight were purchased from the Animal Center of PLA General Hospital and maintained under control temperature (22–23 °C) and light (12:12 h light–dark cycle) at the animal center. The mice were randomly assigned to the following groups. All the animals were ear tagged and randomly grouped by computer. Start with any number in the random number table and obtain N random numbers sequentially in the same direction. The remainder is obtained by dividing the random number by the number of groups, and if it is divided, the remainder is obtained by the number of groups. Finally, group by remainder. All mice were anesthetized with 1% pentobarbital before undergoing surgery and sampling. Briefly, mice were grouped and anesthetized with unilateral renal ischemia/reperfusion injury (uIRI) through 35 min of left renal pedicle clamping. A thermostatic pad kept the mouse's body temperature during surgery. The kidneys were observed to ensure blood flow after removing the clip. To investigate the renal pathological changes and mitochondrial dynamics at different time points after AKI. Euthanization and sample collection were performed at 2, 7, 14, or 28 days. Then, the primary observation time point was designated as 14 days. Next, we investigated the specific role of HGF secreted by MSC. Generally, mice were divided into four groups: sham, uIRI, uIRI + MSC^{ShNC}, and uIRI + MSC^{ShHGF}, with 6 mice per group. Renal subcapsular injection of 2×10^6

collagen-coated hUC-MSCs (col-MSCs) was given immediately after uIRI and again seven days later for two doses. hUC-MSCs therapy through renal subcapsular injection could facilitate its paracrine effect [16]. The mice were euthanized by cervical dislocation after sampling. All the above operations were performed at the Animal Center of PLA General Hospital. The experimenter does not participate in the assignment process, but only knows the final assignment result. Results evaluation and data analysis were performed by a third party, and at least two researchers were asked to cross-check the analysis results.

Histological staining

Kidney tissues were fixed with 4% paraformaldehyde, embedded in paraffin for immunohistology, frozen in OCT solution for cryosectioning and SA-β-Gal staining, and sectioned at 4 μm.

Masson staining

Renal fibrosis was examined by Masson staining according to the manufacturer's instructions. After paraffin sections were dewaxed, hydrated, and nucleated with hematoxylin semen, they were stained with ponceau for 5–10 min. After soaking with a 2% glacial acetic acid solution, the fibers were colored with aniline blue.

SA-β-gal staining

Fresh cryosections were done with a senescence detection kit (GMS10012.3, GENMED) according to the manufacturer's instructions. The green colored area is the senescence enzyme positive area.

Immunohistochemistry

After rehydration and antigen retrieval, the sections were blocked with peroxidase and 5% goat serum successively before incubation with the following primary antibodies: anti-γ-H2A.X (1:400) (2577, Cell Signaling Technology), anti-Ki67 (1:200) (ab16667, Abcam), anti-Col-I (1:250) (ab270993, Abcam), or anti-Vim (1:250) (ab92547, Abcam) at 4℃ overnight. After the HRP-conjugated secondary antibodies (ZSGB-BIO) were incubated, tissue sections were developed with a DAB Peroxidase Substrate (ZSGB-BIO), counterstained with hematoxylin, and mounted. In addition to blood vessels and connective tissue, darker brown areas are positive.

Immunofluorescence

Briefly, the kidney tissue sections were dewaxed, hydrated, and antigen repaired, and then cells or the tissue sections were permeabilized and subsequently blocked with 5% goat serum. After then, tissue frozen sections or cells were exposed to anti-Tomm20 (1:800) (11802–1-AP, Proteintech), anti-PKA (1:750) (ab76238, Abcam), anti-P16 (1:250) (sc1661, Santa Cruz), anti-Drp1pS637 (1:250) (PA5-101038, Thermo), anti-Fn (1:250) (ab2413, Abcam), or anti-αSMA (1:250) (ab7817, Abcam) overnight at 4 °C, followed by incubation with Cy3- or FITC-conjugated secondary antibodies (Beyotime) at 37 °C for 1 h. The nuclei were counterstained with DAPI. They were viewed under a Leica TCS-SL confocal microscope and captured by Olympus Fluoview. Except for blood vessels and connective tissue, the regions with brighter fluorescence are the positive regions.

Electron microscopy

To analyze mitochondrial structure, 1 m^3 kidney tissue with neat incision edges was fixed with 2.5% glutaraldehyde in phosphate buffer (pH 7.4). After being post-fixed with 1% osmium tetroxide for 1 h, the samples were embedded in Epon812, and ultrathin sections were obtained. The ultrathin sections were stained with uranyl acetate and lead citrate and observed using an H7650 transmission electron microscope (Hitachi, Japan).

ATP detection

After the kidney tissue was sufficiently homogenized, cleaved, and centrifuged, ATP production was determined through the Enhanced ATP Assay Kit (S0027, Beyotime) according to the manufacturer's protocol.

Molecular docking

In this study, we used ZDOCK 3.0.2 to predict the binding pattern of c-MET and PKAP (RKACA) proteins. Before the docking, we obtained the structure files of

(See figure on next page.)

Fig. 1 Unopposed mitochondrial fusion, cellular senescence and fibrosis occur successively in the uIRI murine model. **A** Schematic illustrating the collection of animal specimens at different indicated time points. Unilateral IRI was performed in C57BL/6 mice and euthanized separately on days 0, 2, 7, 14, and 28 (n = 6). **B** Images of Masson staining. Scale bar: 50 μm. **C** Images illustrated the overall distribution of the SA-β-gal-positive cells. Scale bar, 50 μm. **D** Immunofluorescence staining images of the mitochondrial outer membrane (Tomm20). Scale bar, 20 μm. **E** Western blot bands of senescence (upper), fibrosis (middle), and mitochondrial dynamics markers (bottom). **F** Quantitative immunoblot analyses of the above bands. The quantification of phosphor-drp1 (Ser616 or Ser637) was normalized to total-drp1. Data are presented as mean ± SD. $^{**}P < 0.01$; $^{*}P < 0.05$. ns, not significant

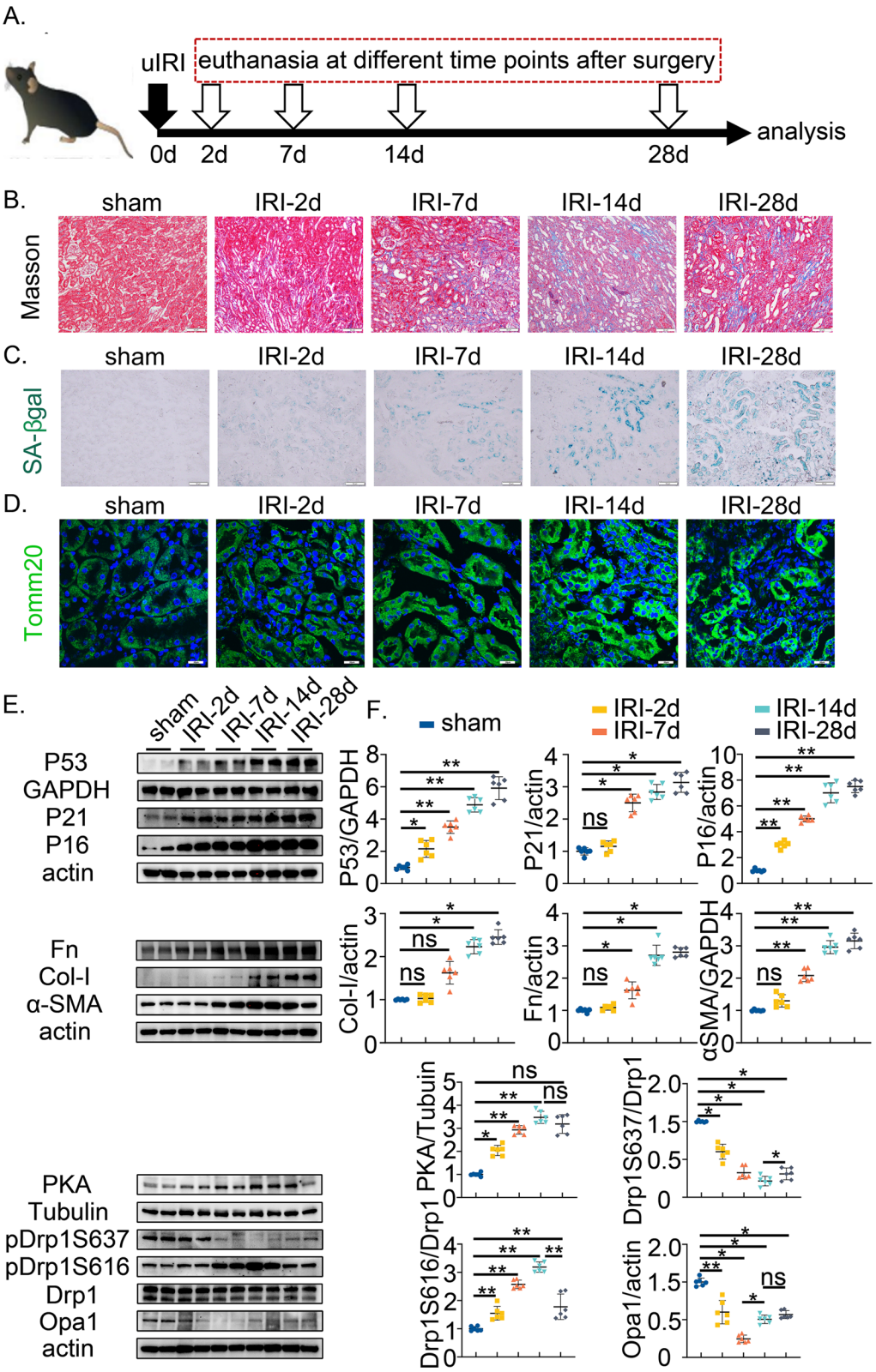

Fig. 1 (See legend on previous page.)

these proteins from the PDB database, and the PDB ids were 3F66 and 6FRX respectively. They were then processed using PyMol2.5.3, including the removal of structural regions with predicted errors.

During the docking, the default configuration of ZDOCK 3.0.2 was used for docking research, and global rigid docking was carried out. After docking, AMBER18 was used for energy minimization under ff14SB force field. Finally, after the energy minimization of protein complex conformation of the use of online tools prodigy binding energy assessment (https://wenmr.science.uu.nl/prodigy/). The binding mode based on the optimal binding energy was visualized by PyMOL 2.5.3.

Cell culture and treatment

Cell culture

HK-2 cells were maintained in DMEM/F12 (Gibico) containing 10% serum in a cell incubator containing 5% CO2 at 37 °C. The cells were then seeded to reach 30% confluence by the next day and exposed to 1% concentration of CO2 at 37 °C for 72 h to mimic chronic hypoxia.

Collection of stem cell–conditioned medium and neutralization with antibody

hUC-MSCs were obtained from Vcanbio Cell & Gene Engineering Corp., Ltd. (Tianjin, China) and cultured in a suitable medium (YOCON Biology, Beijing, China). According to the manufacturer's instructions, the supernatants were collected and concentrated using a Sartorius centrifugal filter. The stem cell-conditioned medium (MSC-CM) was stored at −80 °C until use. Neutralizing antibodies against HGF (AF294, RD) or cMet (AF276, RD) were added to the conditioned medium at a dilution ratio of 1:500 and used to treat HK-2 cells.

Collagen matrix preparation

3 mg/ml rat tail collagen I (Life Technologies) was used to colonize hUC-MSCs under the renal capsule. Rat tail collagen I and sterile 10×phosphate-buffered saline (PBS) was mixed in a 9:1 ratio on ice. Adding 1 M NaOH was used to adjust the pH to 7.4. 2×10^6 adherent hUC-MSCs were resuspended in 80 µl of the above working solution to obtain collagen matrix-encapsulated hUC-MSCs (Col-MSCs).

Lentivirus infection of HGF

To knock down HGF expression, 4×10^5 hUC-MSCs were seeded into a 60-mm dish and transfected with a lentivirus purchased from HanBio Technology or negative control (NC) at an MOI of 60 for 8 h. The cells were incubated for 72 h and then screened with 8ug/ml of puromycin.

Plasmid transfection of PKA

To overexpress PKA, HK-2 cells were seeded to reach 70%confluence for 24 h, then transfected with PKA plasmid using a Lipofectamine 3000 reagent (Invitrogen) according to the manufacturer's instructions. PKA plasmid was purchased from Gene Pharma Bio Inc. The overexpression of protein level was verified by western blot.

Activation of PKA

To improve the enzyme activity of PKA, HK-2 cells were stimulated with 5uM 8-bromo-cAMP (8-Br-cAMP) (S7857, Selleckchem) after the cells had reached a 30% confluence.

Measurement of intracellular cyclic AMP

Briefly, 3×10^5 cells were washed with PBS and lysed with 0.1 mM hydrochloric acid for 20 min at room temperature. After centrifuging, the supernatants were used to measure intracellular cyclic AMP (cAMP) levels using the cAMP ELISA Kit (581001, Cayman Chemical) following the manufacturer's instructions.

Measurement of HGF secretion

Briefly, after centrifuging, the supernatants from hUC-MSCs (passage 6) were used to measure the concentration of human HGF by using the ELISA kit (VAL168, Novus) according to the manufacturer's instructions.

Live cell staining

The following fluorescence images were viewed under a Leica TCS-SL confocal microscope and captured using a confocal microscope (Olympus Fluoview) in less than two hours. The results were obtained from at least three repeated experiments.

(See figure on next page.)

Fig. 2 hUC-MSCs can alleviate renal interstitial fibrosis and renal senescence after AKI. **A** Schematic diagram of treatment. hUC-MSCs were mixed with collagen matrix and given to uIRI mice for two doses. Model group mice were injected with rat tail collagen. Kidneys were harvested at 14 days post-uIRI for analysis (n = 6 mice per group). **B** Immunohistological staining images of Masson staining. Scale bar, 20 µm. **C** Immunohistological staining images of SA-β-gal. Scale bar, 20 µm. **D** Western blotting of senescence indicators. **E** Quantification of senescence indicators. Data are presented as mean ± SD. $^{**}P < 0.01$; $^{*}P < 0.05$. ns, not significant

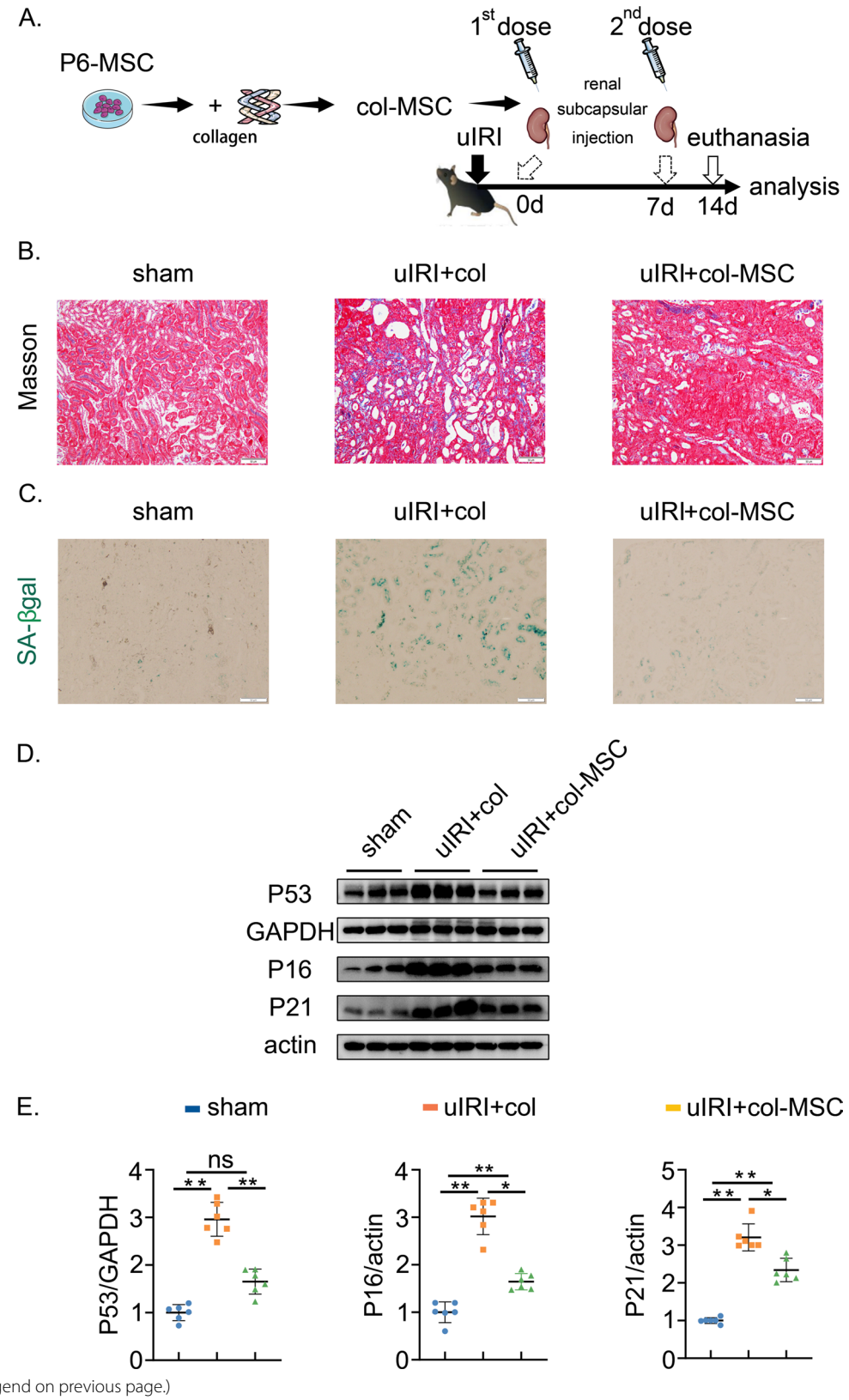

Fig. 2 (See legend on previous page.)

Measurement of intracellular and mitochondrial ROS levels

To detect cellular ROS levels, HK-2 cells were stained with 50 μM 2′,7′-dichlorodihydrofluorescein diacetate (DCF-DA) (S0033, Beyotime) for 45 min and then harvested. ROS up was used as a positive control. Cells were harvested and stained with the mitochondrial superoxide indicator MitoSOX Red (5 μM) (MT14, Dojindo) to measure the mitochondrial ROS levels for 45 min.

Mitotracker staining and analysis of mitochondrial morphology

HK-2 cells were cultured on glass coverslips and stained with 100 nM MitoTracker Green (M7514, Thermo). At least 200 cells were captured, and the mitochondrial morphology was categorized into fragmented, intermediated, and elongated morphotypes. The ratio of elongated mitochondria was calculated.

Mitochondrial membrane potential analysis

HK-2 cells were incubated with 1 μg/ml JC-1 dye (C2006, Beyotime) for 40 min to measure the mitochondrial membrane potential and then microscopically analyzed. The ratio of red to green fluorescence represents the level of the mitochondrial membrane potential. Carbonyl cyanide 3-chlorophenylhydrazone (CCCP) was used as a positive control.

Mitochondrial fractionation/subcellular fractionation

Mitochondrial protein was extracted by a kit (C3601, Beyotime). Cells were lysed and centrifuged at 2500 rpm for 20 minutes to remove cell debris. The resulting supernatants were centrifuged at 3000 rpm for 8 minutes to remove the cell debris and nuclear fraction altogether, after which the supernatants were centrifuged at 11000 g for 30 minutes on ice. The resulting supernatants (cytosolic fraction) were stored on ice, and the pellets were washed once in lysis buffer and then lysed in RIPA buffer (mitochondrial fraction). The extracted fraction was used for western blotting. The GAPDH level was monitored as a cytosol internal loading control. COX IV is used as a mitochondrial internal loading control.

Western blot analysis

Tissues or Cells were lysed in RIPA buffer (P0013B, Beyotime) and determined by Pierce BCA protein assay kit (23225, Thermo) for protein concentration. SDS-PAGE electrophoresis was performed after loading the same amount of protein in each lane. The antibodies required for the experiment are listed as follows. Including anti-P16 (ab51243, Abcam), anti-P21 (ab109520, Abcam), anti-p53 (2524, Cell Signaling Technology), anti- CoxIV (AG8011, Beyotime), anti-PKA Cα (24503–1-AP, Proteintech), anti-Drp1 (12957-1AP, Proteintech), anti-Drp1 pS637 (PA5-101038, Thermo), anti-Drp1pS616 (AF8470, Affinity), anti-CREB (12208–1-AP, Proteintech), anti-CREB pS133 (28792–1-AP, Proteintech), anti-Col-I (ab270993, Abcam), anti-Fn (ab2413, Abcam), anti-α-SMA (ab7817, Abcam), anti-vim (ab92547, Abcam), anti-IL-6 (12912, Cell Signaling Technology), anti-IL-1β (ab9722, Abcam), anti-TNFα (3707, Cell Signaling Technology), anti-Opa1 (66583-1Ig, Proteintech). The actin, GAPDH, or Tubulin level was monitored as a total protein internal loading control. All western blot analyses were repeated three times. The band intensities were quantified using densitometry and ImageJ software. The relative band intensities of Drp1 pS637 over total Drp1 were calculated after normalizing the band intensities to the actin loading control, and the results are presented as the mean with SD.

RNA extraction and real-time PCR

Kidney tissues or cells were homogenized in subsequent processing. After trizol cracking, chloroform extraction, isopropyl alcohol precipitation and 75% ethanol dissolution, we obtained qualified total RNA. To measure mRNA, 1 μg RNA was reversely transcribed using a cDNA Reverse Transcription Kit (Takara), and real-time PCR was performed using SYBR Green PCR Master Mix (Takara) according to the manufacturer's protocol. β-Actin or GAPDH was used for normalization. The quantification was done using ΔCt values.

(See figure on next page.)

Fig. 3 HGF deficiency in hUC-MSCs fail to effectively inhibited renal interstitial fibrosis in uIRI mice. **A** Schematic diagram of treatment. HGF-deficient hUC-MSCs (MSC^{ShHGF}) and negative control cells (MSC^{shNC}) were constructed by lentivirus transfection. C57BL/6 mice were subjected to renal uIRI surgery immediately, followed by renal subcapsular injection of collagen matrix-encapsulated-MSCs (Col-MSC^{ShHGF}) in the treatment group. Two doses of hUC-MSCs were given by subrenal capsular transplantation every 7 days. Control and model group mice were injected with rat tail collagen vehicle and Col-MSC^{shNC}, respectively. Kidneys were harvested at 14 days post-uIRI for analysis (n = 6 mice per group). **B** The ELISA of human HGF in hUC-MSCs-CM passage 6 (P6) showed much higher HGF secretion than HK-2 cells at 36 h. **C**, **D** Western blotting and corresponding quantification showed that the expression level of HGF in MSC^{ShHGF} was much lower than in $MSC.^{shNC}$ of passage 6. **E** Immunohistological staining images of Masson staining (upper, Scale bar, 50 μm). **F** Immunofluorescence of fibronectin (Scale bar, 20 μm). **G** Immunohistochemistry of collagen-I. (Scale bar, 50 μm). **H** Immunohistochemistry of vimentin (Scale bar, 50 μm)

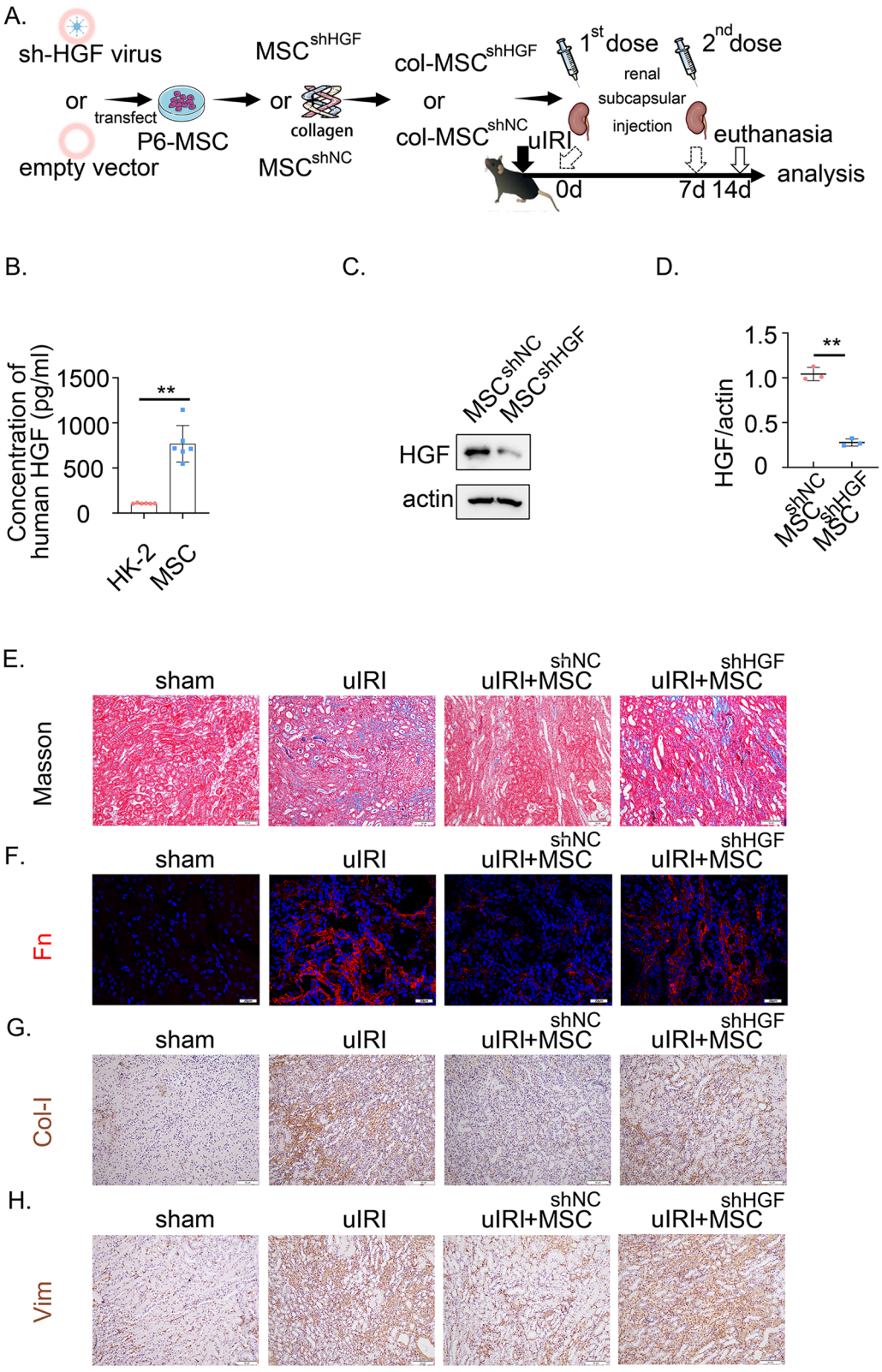

Fig. 3 (See legend on previous page.)

Statistical analysis

Data expressed as mean ± SD are representatives of at least 4–6 experiments in animals and 3 in cells. Statistical analysis was performed using GraphPad Prism 8.0. Significant differences were calculated using an unpaired, 2-tailed t-test between 2 groups and one or two-way ANOVA with multiple comparisons in multiple groups. A P value of less than 0.05 was considered significantly different.

Result

Unopposed mitochondrial fusion participates in the crosstalk of cellular senescence and fibrosis in post-AKI

To investigate the connection among renal senescence, interstitial fibrosis, and mitochondrial dynamics changes after AKI, a robust murine model mimicking unilateral renal ischemia/reperfusion injury (uIRI) was used to analyze at different time points (Fig. 1A). The progression of post-AKI and the accompanying cellular senescence were characterized [3]. Masson staining revealed a steady increase in renal interstitial fibrosis, peaking on day 14 and reducing by day 28 due to severe renal atrophy (Fig. 1B). The SA-β-gal activity increased on the 2nd day and was primarily found in the proximal renal tubular epithelial cells (RTECs) (Fig. 1C). Western blotting analysis further indicated a successive upregulation of cellular senescence marker (p53, p21, p16) and fibrosis marker (fibronectin, collagen-I, and α-SMA) were successively up-regulated as time advanced Fig. 1E, F Upper and Middle). Meanwhile, a time-dependent increase of Tomm20 was detected by immunofluorescence assay (Fig. 1D). Tomm20 is a mitochondrial outer membrane marker and additionally exhibits high mitochondrial content that accumulates due to damaged mitochondria. Unopposed mitochondrial fusion was observed, with a transition from excessive fission to fusion or elongation. Protein kinase A (PKA) increased until reached a plateau on day 14, showing the activated elongation signaling. Drp1pSer637 initially decreased but then upturned from day 14, showing a time-dependent altered expression opposite to Drp1pSer616 and similar to Opa1 (Fig. 1E, F Bottom). Briefly, renal senescence is linked to imbalanced mitochondrial dynamics in progressive renal fibrosis.

Previous research has demonstrated that senescent RTECs could activate renal fibroblasts[3]. Chronic hypoxia is an inherent pathophysiological characteristic of chronic kidney disease post-AKI [17]. In our study, to further investigate the effect of chronic hypoxia on RTECs and its potential contribution to renal fibrosis. Chronic hypoxia [18] was used to mimic the in vivo environment of post-AKI (Fig. S1 A). Specifically, 72 h chronic hypoxia increased the mRNA expression of pro-fibrotic and pro-senescent secretory factors in HK-2 cells, including PDGF, TNF-α, and IL-6 (Fig. S1 B). Through western blotting (Fig. S1 C) and immunofluorescence staining, we found that a series of fibrotic biomarkers (fibronectin, collagen-I, and α-SMA) were up-regulated in NRK-49F upon stimulation with senescent supernatant from HK-2 cells (Fig. S1 D). Briefly, the secretion of senescent RTECs could activate fibroblasts, transforming them into myofibroblasts, a hallmark of renal interstitial fibrosis in post-AKI.

hUC-MSCs can alleviate renal interstitial fibrosis and renal senescence after AKI

To determine the treatment efficacy of hUC-MSCs (Fig. 2A), renal fibrotic and senescent level was detected by Masson staining and SA-β-gal activity respectively. For Masson staining, fibrotic deposition was significantly increased in the uIRI + col group but decreased in uIRI + col-MSC (Fig. 2B). Additionally, the SA-β-gal activity was also found increased in the uIRI + col group but decreased under hUC-MSCs treatment (Fig. 2C). Protein level of senescence markers (p53, p16 and p21) were increased in the uIRI + col group but reversed in the uIRI + col-MSC group (Fig. 2D–E). Overall, our findings demonstrate that hUC-MSCs can alleviate renal interstitial fibrosis and senescence.

Inhibition of HGF secretion from hUC-MSCs ineffectively curbs cellular senescence and renal fibrosis

Additionally, the SA-β-gal activity was found to decrease under hUC-MSCs treatment. HGF knockdown weakened the reduction of SA-β-gal activity (Fig. 4A). Furthermore, γ-H2AX, an indicator of senescence-associated aberrant chromatin, declined in the uIRI + MSC^{ShNC} group while increasing in the uIRI + MSC^{ShHGF} group (Fig. 4B). Ki-67, as a representative index of proliferation,

(See figure on next page.)

Fig. 4 HGF deficiency in hUC-MSCs ineffectively control renal senescence. Grouped according to the experiment in Fig. 3A (n = 6 mice per group). **A** Immunohistochemical images of SA-β-gal. Scale bar, 50 μm. **B** Immunohistochemical images of γ-H2AX. Scale bar, 50 μm. **C** Immunohistochemical images of Ki-67. Scale bar, 50 μm. **D** Relative mRNA expressions of pro-fibrotic and pro-senescent secretory factors, including PDGF, TGF-β, and IL-1β. **E** Immunoblots of senescence indicators (p53, p16) and pro-fibrotic and pro-senescent secretory factors (IL-1β, TNF-α, and IL-6). **F** Relative bands intensity of senescence level. Data are presented as mean ± SD. $^{**}P < 0.01$; $^{*}P < 0.05$. ns, not significant

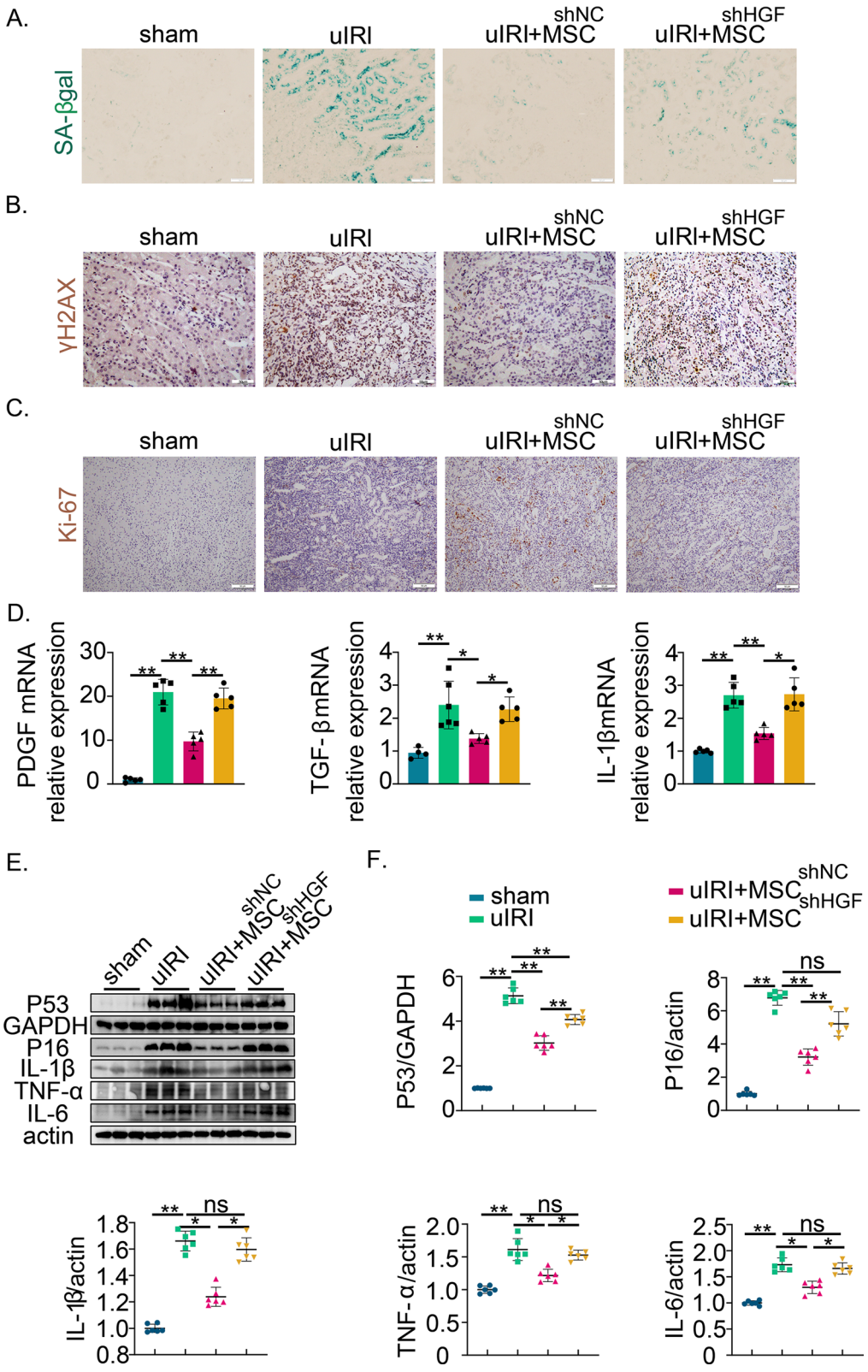

Fig. 4 (See legend on previous page.)

showed the opposite trend to γ-H2AX (Fig. 4C). Protein and mRNA expression of pro-fibrotic and pro-senescent secretory factors was measured (Fig. 4D). Western blotting analysis showed significantly increased expression of senescence markers (p53 and p16) in the uIRI group. It was decreased under hUC-MSCs treatment and reversed in the uIRI + MSC^{ShHGF} group (Fig. 4E–F). Overall, our findings demonstrate that HGF deficiency has impaired hUC-MSCs therapeutic ability for cellular senescence and renal fibrosis.

HGF-derived hUC-MSCs rescue mitochondrial dysfunction

The above studies mentioned that HGF could reverse the down-regulation of p53 and senescence mediated by hUC-MSCs. It is, therefore, reasonable to consider hUC-MSCs-derived HGF as a regulator of p53-induced cellular senescence, for which mitochondrial elongation is responsible [8]. Mitochondrial dynamics change affected by HGF-mediated hUC-MSCs in renal senescence alleviation was further explored. Renal ATP preservation was lower in the uIRI + $MSCSh^{HGF}$ group than in the uIRI + MSC^{ShNC} group (Fig. 5A). Using a transmission electron microscope, different mitochondrial morphology was first exhibited for hUC-MSCs transplantation in uIRI groups (Fig. 5B). Mitochondrial morphology was uniform in the sham group and fragmented in uIRI group. After treatment with MSC^{shNC}, which generally secretes HGF, mitochondria recover to an appropriate uniform length. However, after treatment with MSC^{shHGF}, which does not secrete HGF properly, the mitochondria appear to be more elongated and have fine filaments. Mitochondrial elongation is based on the longitudinal length of mitochondria and the transverse width. We found that the transverse width of mitochondria was significantly shortened after the MSC^{shHGF} treatment compared to the MSC^{shNC} treatment. To put it bluntly, the ratio of longitudinal and transverse diameters of mitochondria was significantly upregulated. Interestingly, lipid droplets were observed around overstretched and fragmented mitochondria in the uIRI group. Immunofluorescence double staining for p16 and Tomm20 further supported the curative role of HGF in renal senescence related to mitochondrial dysfunction (Fig. 5C).

Kim YY et al. first reported in 2020 that p53 could regulate PKA-Drp1pS637 signaling [8]. However, since the cell membrane protein cMet is difficult to co-localize with the nuclear transcription factor p53, the interaction between cMet and PKA signaling is more reasonable. In addition, PKA controls cell cycle-related spindle formation by regulating Drp1pS637 signaling [19]. Cell cycle arrest associated with abnormal spindle formation is also an important cause of cell senescence. Therefore, the link between MSCs-derived HGF and PKA-Drp1pS637 signaling was directly investigated. Immunofluorescent detection demonstrated that the up-regulation of PKA expressed in uIRI was suppressed by hUC-MSCs transplantation but reversed by HGF knockdown in hUC-MSCs (Fig. 5D). Following western blotting analysis affirmed that HGF-secreted hUC-MSCs could reverse the over-expressed PKA in the uIRI group (Fig. 5E–F).

To further complete the chain of evidence for the MSCs-derived HGF-cMET-PKA-DRp1ps637 signaling axis, the molecular docking pattern of cMet, the putative receptor of HGF, with PKA was supplemented in Fig. 5G. The results showed that cMet had a strong binding potential with PKA. The binding energy of cMet-PKA is -12.1 kcal/mol. Hydrogen bonding and salt bridge during the formation of cMet-PKA (PRKACA) complex can be seen in Fig. 5G. For example, Q1304, D1310, V1178, K1179, F1341, Y1349 on cMet protein and K266、R270、Y229、R256、K249 on PKA protein form hydrogen bonding (Fig. 5G). Hydrogen bonding is the main interaction force between cMet protein and PKA protein. Hydrogen bonding is an important non-covalent binding and is very important for protein–protein electrostatic complementation. Many hydrogen bonding actions indicate that the cMet-PKA obtained by our docking has a strong bonding effect. Molecular docking demonstrated the binding potential of c-Met and PKA, and confirmed the regulation of HGF on mitochondrial elongation driven by PKA. Therefore, the treatment efficacy of hUC-MSCs-derived HGF in senescence alleviation correlated with imbalanced mitochondrial dynamics.

(See figure on next page.)

Fig. 5 HGF-deficient MSCs exerts insufficient mitochondrial protection in uIRI mice. Grouped according to the experiment in Fig. 3A (n = 6 mice per group). **A** Quantification of ATP level in kidney tissue. **B** Electron microscopy images. (× 15 000 magnification). Red arrows indicate typical mitochondrial morphological changes. The accumulation of lipid droplets appeared around both stretched and fragmented mitochondria in the uIRI group. The mitochondria were significantly elongated in the uIRI + MSC^{HGF} group. Blue arrows indicate lipid droplets. Scale bar, 2 μm. **C** Immunofluorescence images of P16 (green), Tomm20 (red), and DAPI (blue). Scale bar, 20 μm. **D** Images of immunofluorescence showing the expressions of PKA (red) and DAPI (blue). **E** Immunoblot images of PKA. **F**) Quantitative immunoblot analyses of PKA. **G** The binding pattern of the cMet-PKA (PRKACA) complex, shown in wheat color as cMet and blue as the target PKA protein. The dashed yellow line shows hydrogen bonding. Data are presented as mean ± SD. $^{**}P < 0.01$; $^{*}P < 0.05$. ns, not significant

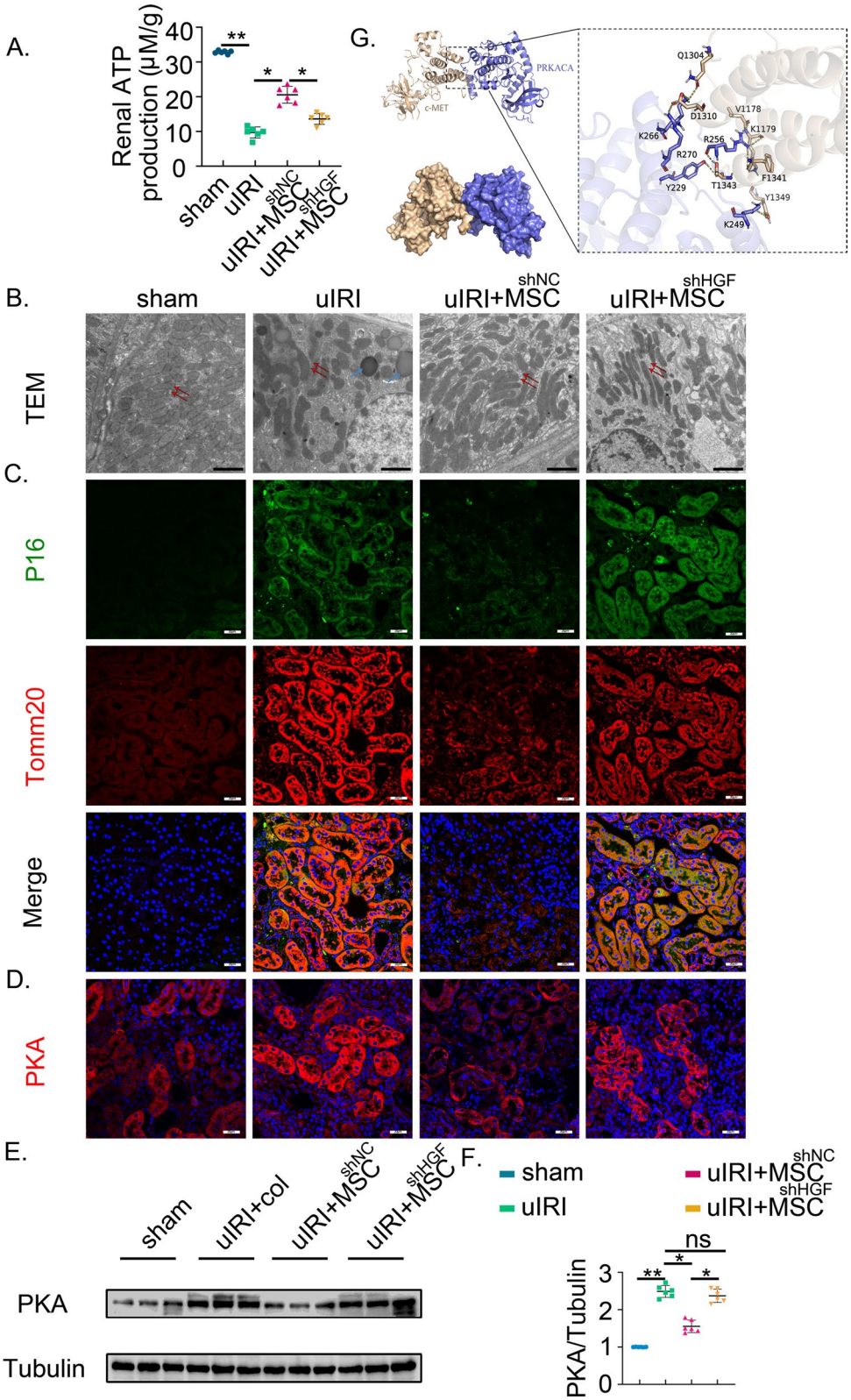

Fig. 5 (See legend on previous page.)

hUC-MSCs-released HGF regulates mitochondrial elongation in RTECs via cMet

Next, to understand the mechanism of hUC-MSCs-derived HGF in mitochondrial elongation in RTECs, the hypoxic HK-2 cells model described in the previous section was employed to culture with MSC-CM (Fig. 6A). Cellular ROS levels, a mediator of senescence, were reduced in hypoxic HK-2 cells treated with MSC-CM compared to untreated ones (Fig. 6B). The co-expression of p16 and α-SMA in hypoxic HK-2 cells confirmed the anti-senescent effect of hUC-MSCs-derived HGF (Fig. 6C). P53 and PKA are upregulated during chronic hypoxia and reversed by MSCs treatment. However, blocking HGF with antibodies does not effectively curb their upregulation, even when other cytokines are still present in MSCs (Fig. 6D–E). These results indicated that MSCs-derived HGF had a crucial inhibitory effect on p53 and PKA. Moreover, the p53-PKA signal axis has been shown to induce cellular senescence in previous studies [8], suggesting that MSCS-derived HGF has a senescent effect. Compared with the control group, the mitochondrial fusion proteins MFN1, MFN2, Opa1, and Drp1pS637 were inhibited due to increased mitochondrial fission caused by chronic hypoxia. The mitochondrial fusion proteins were upregulated after treatment with MSCs that normally secreted diverse cytokines. However, blocking HGF with antibodies alone can lead to a relative imbalance in fission–fusion. Mitochondrial fusion proteins remain up-regulated, and mitochondrial length cannot be effectively controlled within the appropriate range. In theory, the dynamic changes of p53, PKA, and mitochondrial fusion proteins showed the same trend in each group. In practice, theoretical results were obtained when comparing the MSCs treatment with the HGF blocking. This suggests that the PKA-Drp1pS637 signal axis is only active when it receives HGF stimulation from MSCs. The reason for the inconsistent changes of the above signals in other groups may be that the Drp1pS637 signal is also regulated by other upstream, such as AKT [20] or GSK3β [21]. Moreover, mitochondrial dynamics is a dynamic balance of fission and fusion rather than a simple combination of the two events. "Beyond is as wrong as falling short." Therefore, chronic hypoxia-induced mitochondrial fission cannot be effectively treated by HGF-deficient MSCs. On the contrary, it may lead to the elongation of fission-deficient mitochondria and, thus, over-upregulation of fusion-related proteins. The cells are still viable but exhibit senescence.

cMet, the known receptor for HGF, was considered for the anti-senescence effect [22] (Fig. 7A). Adding the cMet antibody has a similar effect to HGF neutralization in inducing the expression of P53, vimentin, PKA, and Drp1pSer637 (Fig. 7B, C). Moreover, it has been observed that the cMet exerts a significant impact on the mitochondrial level, as evidenced by mitotracker (Fig. 7D, E), superoxide level (Fig. 7F), and membrane potential (Fig. 7G). Following oxygen deprivation, the mitochondria exhibited a more fragmented and prolonged morphology than the control group. Treatment of MSC-CM ameliorated the homogeneity of mitochondrial morphology. Nevertheless, neutralization by cMetAb resulted in elongated mitochondria, which exhibited an interconnected network structure (Fig. 7D). The above observations revealed that MSCS-derived HGF can inhibit PKA signaling through the receptor cMet, thereby preventing the excessive upregulation of Drp1pS637 signaling and mitochondrial elongation. In brief, imbalanced mitochondrial dynamics were rectified by hUC-MSCs-derived HGF in RTECs.

Up-regulation of PKA restores excessive mitochondrial elongation in RTECs

Excessive mitochondrial elongation in cellular senescence is regulated by PKA [8]. To further investigate the relationship between PKA and Drp1pSer637 in regulating mitochondrial elongation, PKA activation or overexpression was performed in hypoxic HK-2 cells within MSC-CM (Fig. 8A). A marked decrease in intracellular cAMP level, a potent inducer of PKA activity, was observed when treated with MSC-CM under chronic hypoxia, indicating that the enzymatic activity of PKA was inhibited under HGF secretion (Fig. 8B). Therefore, whether PKA enzyme activity participates in mitochondrial length control of hUC-MSCs-derived HGF was further explored. When hypoxic HK-2 cells were treated with MSC-CM, the

(See figure on next page.)

Fig. 6 hUC-MSCs-derived HGF regulates mitochondrial dynamics in RTECs. **A** Schematic diagram of treatment. MSC-CM: conditioned medium collected and concentrated from hUC-MSCs. OD: 72 h of oxygen deprivation. HGFAb: neutralizing antibody of human HGF. HK-2 cells were grouped according to the plus sign as shown for treatment (n = 3 experiments). Cells were incubated with MSC-CM with HGFAb under hypoxic conditions and harvested for morphological and immunoblot analysis. **B** Typical images of total intracellular reactive oxygen species production in cells loaded with DCF-DA probes. **C** HK-2 cells were immunostained with p16 (red) and α-SMA (green) to show confocal images. Scale bar, 20 μm. **D** Western blot bands of senescence, fibrosis, and mitochondrial dynamics. **E** Quantitative immunoblot analyses of PKA and phosphor-Drp1ser637. $^{**}P < 0.01$; $^{*}P < 0.05$. ns, not significant

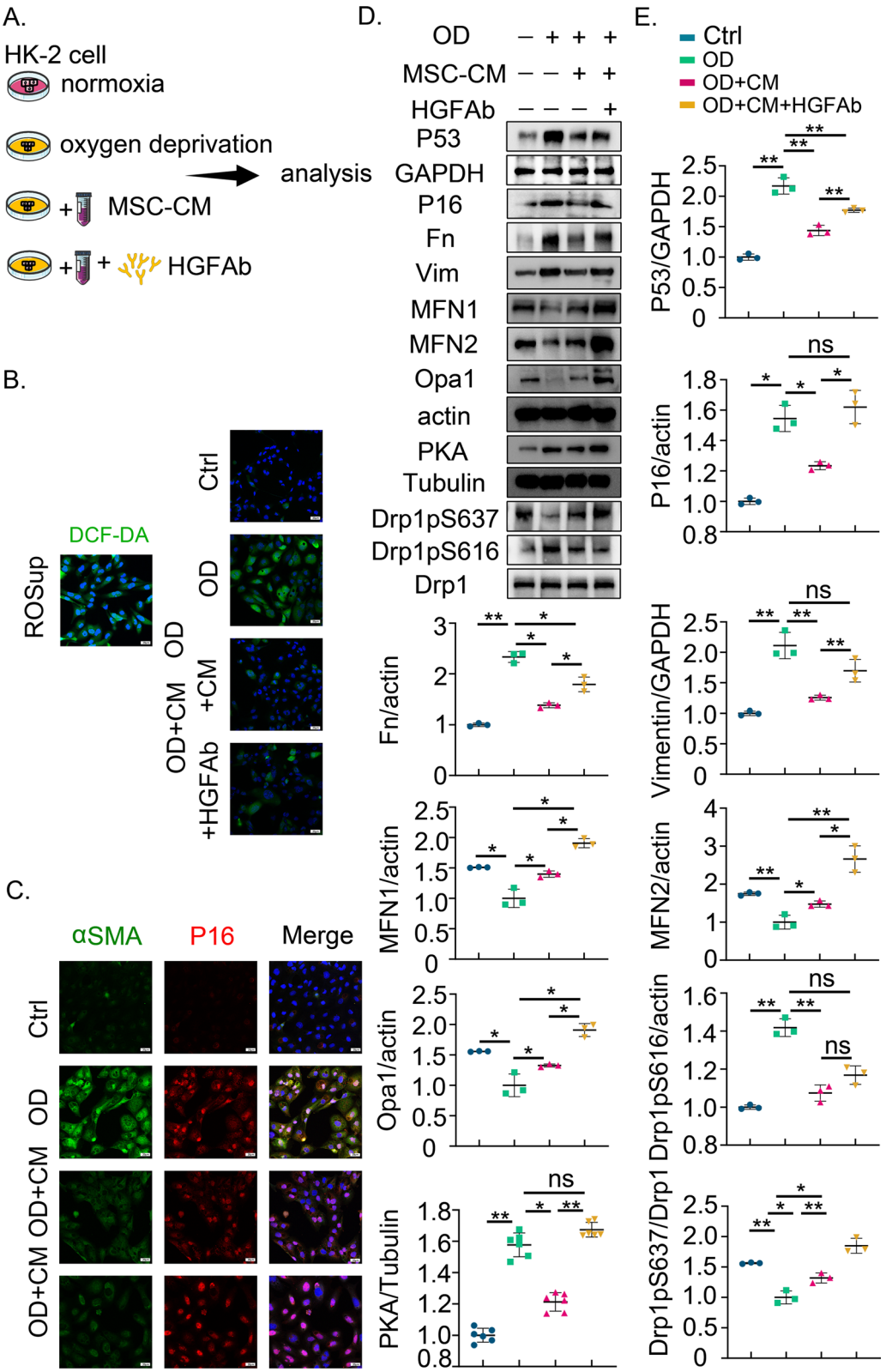

Fig. 6 (See legend on previous page.)

expression of Creb1pSer133, a representative marker for PKA activation, was decreased but up-regulated by the PKA activator despite the PKA protein level remaining unchanged (Fig. 8C). The Drp1pSer637 and P16 expression levels were also increased in PKA activator treatment (Fig. 8C, D), showing that mitochondrial elongation and cellular senescence were induced by PKA enzyme activity. Additionally, in hypoxic HK-2 cells treated with MSC-CM, activation of PKA significantly prolonged mitochondria (Fig. 8E, F). In order to confirm the Drp1 subcellular position, isolation of cytoplasmic and mitochondrial proteins showed that the expression of Drp1 in cytoplasm was higher than that in mitochondria (Fig. 8G). DRP1 retains largely in the cytoplasm and thereby limits mitochondrial fission, providing solid evidence for uncontrolled mitochondrial elongation.

To determine if the PKA protein level is necessary for the increasing Drp1pSer637 level, experiments were conducted under stable expression of Creb1pSer133 (Fig. 9A). An observable increase in Drp1pSer637 expression was affected by up-regulated PKA protein (Fig. 9B, C), which indicates excessive mitochondrial elongation. Using mitotracker staining, we found that treating HK-2 cells with MSC-CM under hypoxic conditions significantly prolonged mitochondria after PKA overexpression (Fig. 9D, E). Additionally, in hypoxic HK-2 cells treated with MSC-CM, the expression of Drp1 was down-regulated in mitochondria under PKA overexpression (Fig. 9F). DRP1 retains in the cytoplasm, consistent with PKA activation, finally promote mitochondrial elongation.

To comprehensively understand the overall mechanism, a proposed model was presented in Fig. 10. Our graphic summary emphasizes the importance of renal tubular senescence in ischemia–reperfusion injury and the mitochondrial therapeutic potential of HGF secreted by hUC-MSCs. Furthermore, our work highlights the interconnected nature of hUC-MSC therapy, preventing imbalanced mitochondrial dynamics through fusion-based mechanisms. In parallel with inhibition in extensive pathological fission of renal mitochondria, hUC-MSCs restricted the hyperphosphorylation of Drp1 at the Ser637 site, which is secondary to the surge of PKA via HGF secretion. Thereby offering comprehensive protection to the kidneys.

Discussion

In our findings, our study underscores the significant protective impact of HGF, which is released by hUC-MSCs, in shielding against renal senescence and subsequent fibrosis in post-AKI. The absence of HGF weakens the ability of hUC-MSCs to curb excessive mitochondrial elongation, as it restricts hyperphosphorylation of Drp1 at the Ser637 site, resulting from an increase in PKA.

Renal senescence following AKI is a crucial factor in developing progressive fibrosis [23]. Renal senescence and fibrosis often feed into each other and form a vicious cycle in kidney diseases [24, 25], the precise role of mitochondrial dynamics during this process still lacks a clear understanding. Our study has shown their developmental trajectory, as evidenced by the rapid response of mitochondrial dynamics to temporal changes linked to the senescence of RTECs and subsequent renal interstitial fibrosis. Mitochondrial dynamics is associated with cell cycle progression [26], and excessive fusion mediated by mitofusin-2 (MFN2) can block the proliferation of vascular smooth muscle cells [27]. Unopposed fusion, a relatively excessive fusion due to an imbalance in fission and fusion-based mitochondrial dynamics, has been proposed in several studies [28, 29]. This relatively inadequate fission of mitochondrial dynamics leads to uncontrolled mitochondrial elongation. Our study has revealed that mitochondrial dynamics shift from hyper-fission to relative fusion as renal senescence increases after renal ischemia–reperfusion injury. Damaged mitochondria cannot respond rapidly to the dynamic transition in fission and thus cause an unopposed fusion. Uncontrolled mitochondrial elongation then leads to progressive renal senescence, which contributes to the development of renal fibrosis. Previous studies have demonstrated that the senescence of RTECs is an effective therapeutic target against renal interstitial fibrosis [3, 4]. In our research, the activation of fibroblasts by senescent RTECs also confirmed that cellular senescence could bring about renal fibrosis.

(See figure on next page.)

Fig. 7 hUC-MSCs-derived HGF regulates mitochondrial elongation in RTECs via cMet. **A** Schematic diagram of treatment (n = 3 experiments). MSC-CM: conditioned medium collected and concentrated from hUC-MSCs. OD: 72 h of oxygen deprivation. cMetAb: neutralizing antibody of human cMet. **B** Western blot bands of senescence, fibrosis, and mitochondrial signaling. **C** Quantification of PKA and phosphor-Drp1ser637. **D** Images of Mito-Tracker Green staining. Scale bar: 20 μm. Representative different mitochondrial morphologies are shown on the right. Among them, intermediate mitochondria had both punctate fragments and elongated twisted filaments. **E** Quantitative mitochondrial morphology analysis. **F** Images of Mito-Sox Deep Red-labeled mitochondria presented with TOTO-3. Scale bar: 20 μm. **G** Images of JC-1 (Red fluorescence indicates normal membrane potential, and green indicates depolarization). Scale bar: 20 μm. Data are presented as mean ± SD. $^{**}P < 0.01$; $^{*}P < 0.05$. ns, not significant

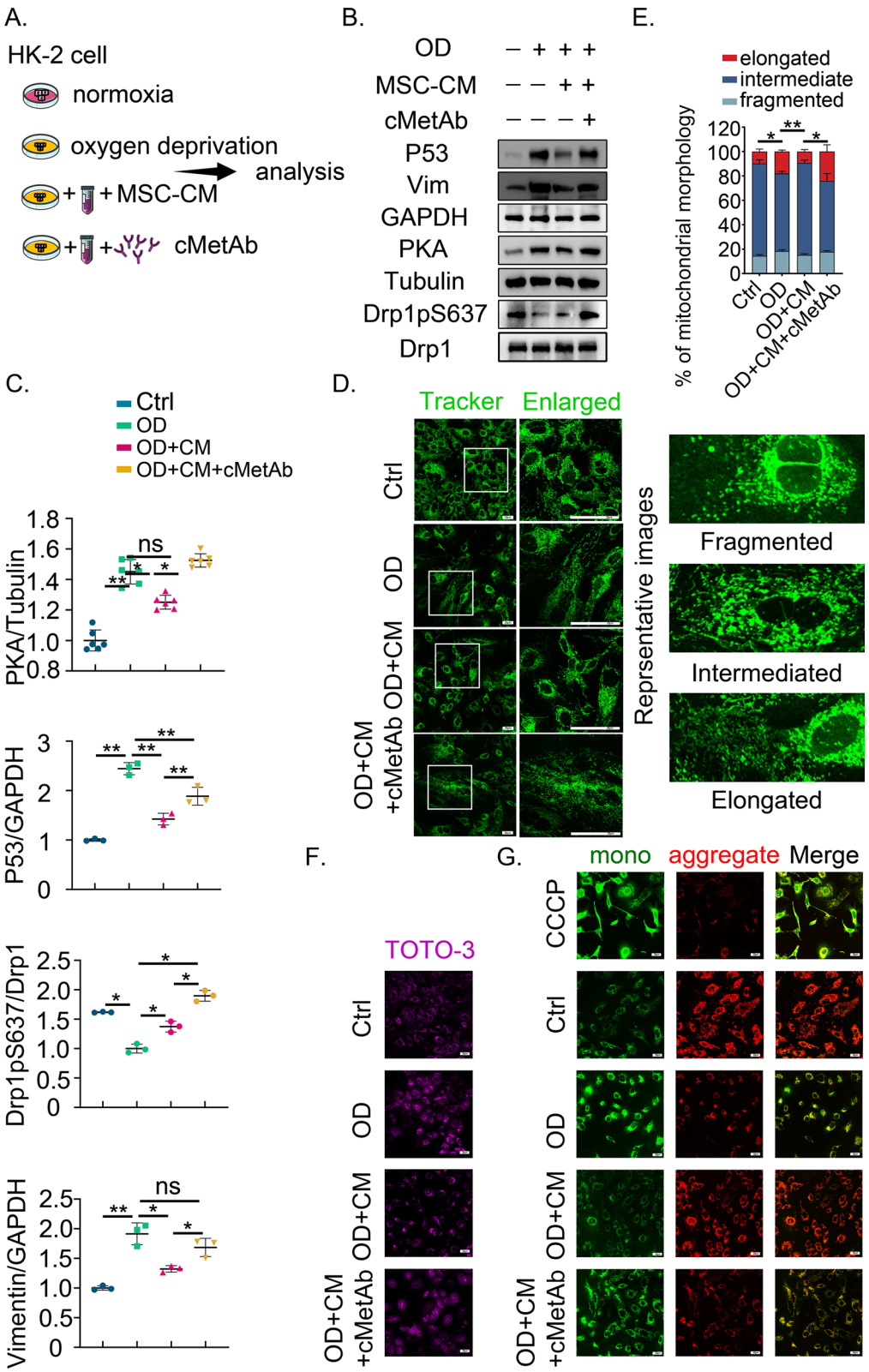

Fig. 7 (See legend on previous page.)

Reports suggest that hUC-MSCs may alleviate renal senescence induced by AKI in rats [11], our research was consistent with that. However, which cytokines secreted by hUC-MSCs are responsible for this effect remains unclear. Hepatocyte Growth Factor (HGF), a classical peptide-containing multifaceted cytokine, has the excellent characteristic of cell-cycle regulation [30]. Our findings reveal that hUC-MSCs secrete HGF, which acts as an anti-senescent factor to halt progressive fibrosis post-AKI. Besides, reactive oxygen species (ROS), considered an essential mediator of senescence [31], have also been inhibited by hUC-MSCs-derived-HGF in our study. Furthermore, the classical tyrosine kinase receptor c-Met, a well-known transmembrane receptor of HGF, exhibits similar effects after neutralizing with antibodies in vitro in our work, further corroborating the treatment ability of HGF.

According to the research, hUC-MSCs possess therapeutic potential for reducing senescence and renal interstitial fibrosis by addressing mitochondrial dysfunction through HGF secretion. Research suggests that lipid metabolism disorders contribute to post-AKI [32], and our study has consistently observed an accumulation of lipid droplets in electron microscopy. Interestingly, the coexistence of fragmented and twisted or elongated mitochondria alongside lipid droplet accumulation around in uIRI was discovered, indicating that extreme morphological changes are linked to renal injury. Mitochondrial morphology homogeneity was improved after hUC-MSCs treatment but disrupted in HGF deficiency, leading to ineffective curb of mitochondrial elongation.

The phosphorylation of Drp1 at Ser637 (Drp1pS637) is involved in various pathological processes, including the regulation of vascular smooth muscle calcification regulated by p53 [33], improper formation of spindle during the cell cycle, cellular senescence [8] regulated by protein kinase PKA [19], or excessive mitochondrial elongation adjusted by GSK3β [34]. However, it has been less reported in kidney diseases. Our current study observed a sequential elevation of PKA and phosphor-drp1Ser637 in post-AKI, suggesting a signaling pathway through which HGF regulates mitochondrial elongation. PKA was first significantly upregulated on day 14 in uIRI mice, while Drp1pS637 remained at low levels due to mitochondrial fission in the acute phase. Drp1pS637 was not gradually upregulated until day 28 when renal mitochondrial fission gradually lost its dominance with decreased Drp1pS616As a downstream signal of PKA, the late-onset upregulation of Drp1pS637 is plausible. The senescence-related PKA-Drp1pS637 signaling axis was ineffective until the chronic phase after uIRI because cellular senescence gradually accumulates in the chronic phase over time after uIRI. Therefore, the changing trend of PKA and Drp1pS637 were not wholly consistent at the same time in the whole kidney. Unlike normoxia, Drp1pS637 was down-regulated, and PKA was reversed after hypoxia in vitro, indicating that hypoxia leads to increased mitochondrial fission (Figs. 6D, 7B, 9C). This is consistent with in vivo experiments. These inconsistent changes may be due to another fact that the Drp1pS637 signal is also regulated by other upstream, such as AKT [20] or GSK3β [21]. Compared with MSCs treatment, blocking MSCS-derived HGF or cMet (recognized receptors for HGF), overexpression or activation of PKA in renal tubular epithelial cells led to significant upregulation of Drp1pS637 under 72 h of chronic hypoxia (Figs. 6D, 7B, 9C). Since the in vitro experiments were mainly performed on the senescent renal tubular epithelium, the changing trend of PKA and Drp1pS637 was consistent. Our study aims to explain how mitochondrial elongation and cellular senescence induced by PKA-Drp1pS637 are involved in the chronic transition of AKI using relative unopposed mitochondrial fusion. Since cellular senescence is one of the various pathologic forms involved in CKD transition after AKI, it is understandable that the upregulation of Drp1pS637 is secondary to, rather than synchronized with, the upregulation of PKA.

To address this issue, we confirmed that HGF released from hUC-MSCs curbs the expression of PKA and drp1S637, and its effect is reversed upon activation or overexpression of PKA. Studies demonstrate that the elevated cAMP and PKA catalytic subunits may be

(See figure on next page.)

Fig. 8 Activation of PKA restores excessive mitochondrial elongation in RTECs. **A** Schematic diagram of treatment. Along with 3 days of chronic hypoxia, HK-2 cells were subjected to PKA activation (8-bromo-Camp) with or without MSC-CM continuously before harvest. Cells were subsequently harvested for morphological and immunoblot analysis (n = 3 experiments). OD: 72 h of oxygen deprivation. MSC-CM: conditioned medium collected and concentrated from hUC-MSCs. 8-br-cAMP: 8-bromo-cAMP. **B** The quantification of intracellular cAMP by ELISA. **C** Western blot of PKA activation at consistent protein expression levels. **D** Quantitative protein expression level of PKA and phosphor-Drp1ser637. **E** Images of Mito-Tracker Green staining. Scale bar: 20 μm. Representative different mitochondrial morphologies are shown below. Among them, intermediate mitochondria had both punctate fragments and elongated twisted filaments. **F** Quantitative mitochondrial morphology analysis of Mito-Tracker staining. **G** Western blot images of cytosolic (cyto) and mitochondrial (mito) drp1 showing its subcellular localization. The GAPDH level was monitored as a cytosol internal loading control. COX IV is used as a mitochondrial internal loading control. After PKA aactivation, drp1 remains in the cytoplasm rather than mitochondria. Data are presented as mean ± SD. $^{**}P < 0.01$; $^{*}P < 0.05$. ns, not significant

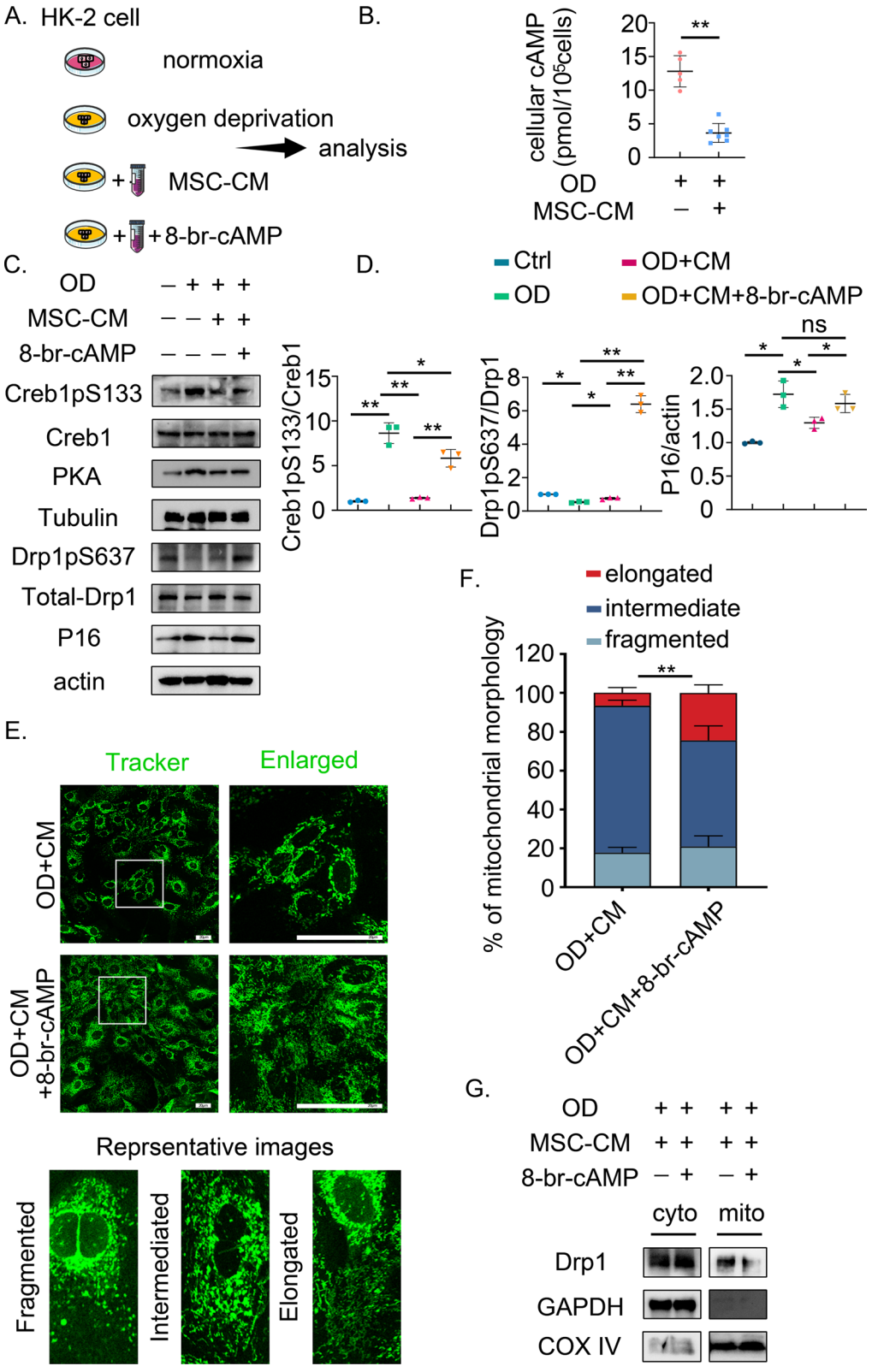

Fig. 8 (See legend on previous page.)

expressed by mitochondrial outer membrane (OMM) targeting, and the disassembly step of Drp1 catalytic cycle was inhibited by Drp1pS637. The accumulation of slowly recycling Drp1 oligomers at the OMM ultimately remodeled the mitochondria into an interconnected reticulum [35]. Our study also confirmed that Tomm20, a known marker for OMM, was unrestricted in HGF-depleted hUC-MSCs-based therapy. Therefore, it is reasonable to speculate that the curb of Tomm20 by secretory HGF leading insufficient space for Drp1 oligomers to accumulate, which may assist PKA and final mitochondrial elongation. In conclusion, the regulation of hUC-MSCs-derived HGF is dominated by PKA-Drp1pS637 signal and supplemented by Tomm20 restriction.

Two studies yielded opposite results on renal fibrosis progression when using mitochondrial fission inhibitor [36, 37]. It is noteworthy that prior research unveiled the promotion of mitochondrial biogenesis (central fission) [13] or autophagic clearance (eccentric fission) [12] by secretory HGF. Discovery of HGF released from hUC-MSCs can suppress fusion-based mitochondrial elongation in our research seems to challenge the idea that inhibiting fission is beneficial [12]. The balance of mitochondrial dynamics may provide a reasonable explanation. Mitochondrial fission includes biogenesis in the form of central symmetric division and mitophagy in eccentric. Mitochondrial biogenesis contributes to sustained healthy cell proliferation, whereas mitophagy removes damaged organelles. However, persistent fission can lead to malignant proliferation or disruption of cell integrity [38]. Mitochondrial fission has causative roles in endothelial senescence [39]. Upregulates Drp1 leading to vascular senescence and atherosclerosis [40]. However, promoting PGC1α-mediated mitochondrial biogenesis can alleviate renal fibrosis and senescence [41]. Enhanced mitochondrial fission in senescent Endothelial progenitor cells also restores the youthful phenotype [42].Mitochondrial fusion, another component of the dynamics balance, can participate in organ growth during development and alleviate cellular damage by diluting mitochondrial fragmentation fragments. However, continuous mitochondrial fusion can lead to elongation, which connects to the formation of giant mitochondria. Such mitochondria have a hyperpolarized membrane potential and produce large amounts of ROS, which can lead to cellular senescence [43]. Fusion, by diluting damaged mitochondria, and fission, by segregating damaged mitochondria, are both beneficial. However, the overloading of either two processes can be detrimental. Fission and fusion are not merely opposing forces. For example, knocking down or overexpressing fission receptors, such as MID51/49 (MIEF1/2), induced significant mitochondrial elongation [44]. Therefore, a delicate dynamics-based balance is more critical than one process. Particularly, interest in excessive fusion-based mitochondrial elongation was addressed because of the hyperpolarized mitochondria produced and the subsequent cellular senescence. Traditional studies have focused on fission overload [12] and neglected fusion. Inhibiting apoptosis caused by excessive fission is beneficial for cell survival but can lead to senescence due to apoptotic resistance. Therefore, maintaining a viable cell state by controlling senescence is also of concern. The present study suggests that hUC-MSCs respond to excessive fission in post-AKI by increasing the fusion level. However, continued fusion, if not checked by hUC-MSCs-derived HGF, may uncontrollably amplify the fusion process, ultimately leading to cellular senescence.

Unfortunately, technical limitations prevented the monitoring of mitochondrial dynamics in post-AKI during our research. Developing 3D mitochondrial dynamic imaging techniques is necessary to reveal specific morphological changes in mitochondria in post-AKI. Additionally, the stretching of mitochondria has been shown to cause changes in the contact sites of other organelles with the mitochondrial membrane. To this end, further research into regulating hUC-MSCs in the interaction between mitochondria and endoplasmic reticulum or cytoskeleton is essential.

(See figure on next page.)

Fig. 9 Overexpression of PKA restores excessive mitochondrial elongation in RTECs. **A** Schematic diagram of treatment. Along with 3 days of chronic hypoxia, HK-2 cells were subjected to PKA overexpression (PKA plasmid) with or without MSC-CM continuously before harvest. Cells were subsequently harvested for morphological and immunoblot analysis (n = 3 experiments). OD: 72 h of oxygen deprivation. MSC-CM: conditioned medium collected and concentrated from hUC-MSCs. PKA-OE: PKA plasmid. **B** Immunoblot of PKA overexpression at consistent enzyme activity. **C** Quantitative protein expression level of PKA and phosphor-Drp1ser637. **D** Images of Mito-Tracker Green staining. Scale bar: 20 μm. Representative different mitochondrial morphologies are shown below. Among them, intermediate mitochondria had both punctate fragments and elongated twisted filaments. **E** Quantitative mitochondrial morphology analysis of Mito-Tracker staining. **F** Western blot images of cytosolic (cyto) and mitochondrial (mito) drp1 showing its subcellular localization. The GAPDH level was monitored as a cytosol internal loading control. COX IV is used as a mitochondrial internal loading control. After PKA overexpression, drp1 remains in the cytoplasm rather than mitochondria. Data are presented as mean ± SD. $^{**}P < 0.01$; $^{*}P < 0.05$. ns, not significant

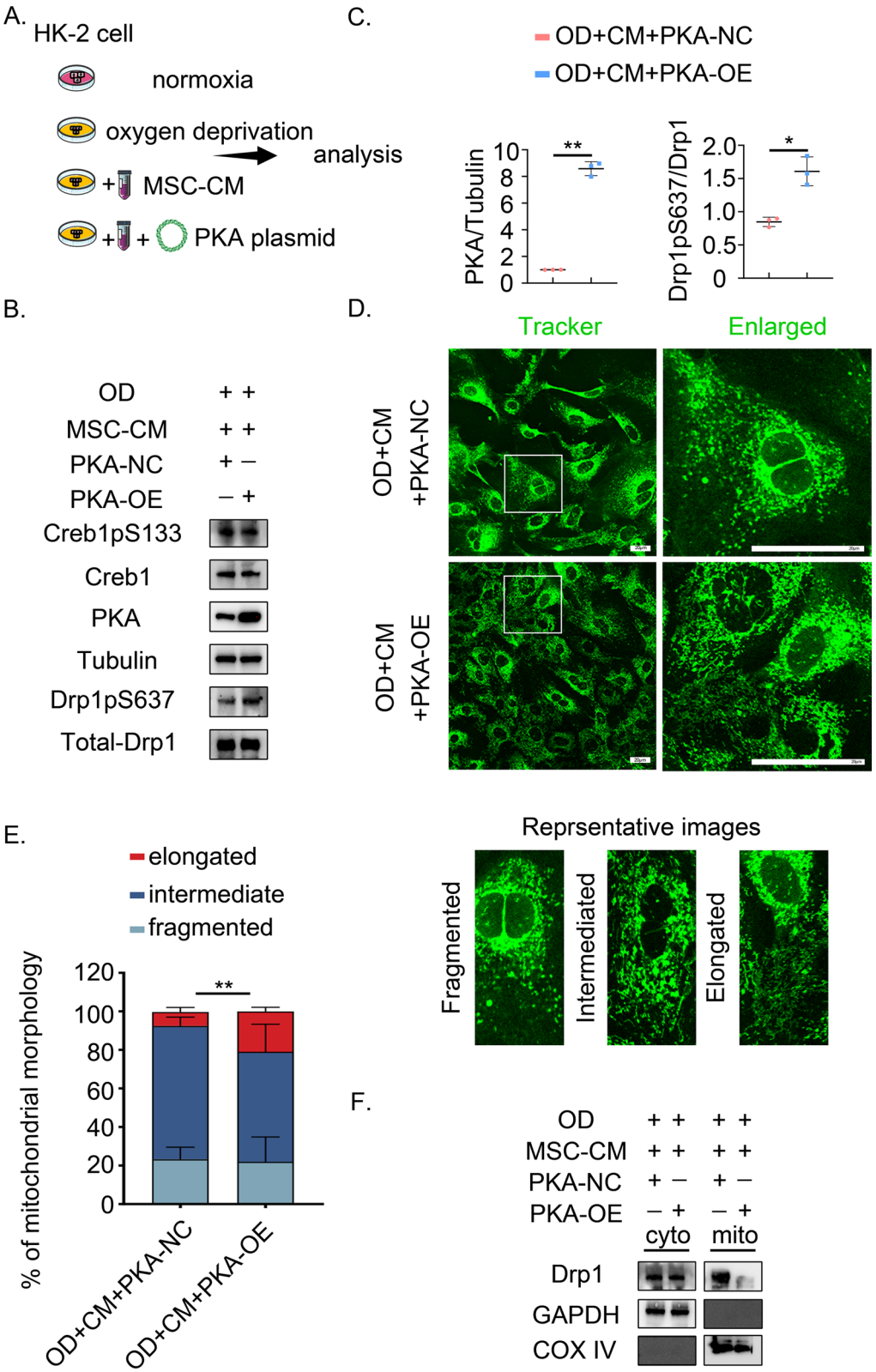

Fig. 9 (See legend on previous page.)

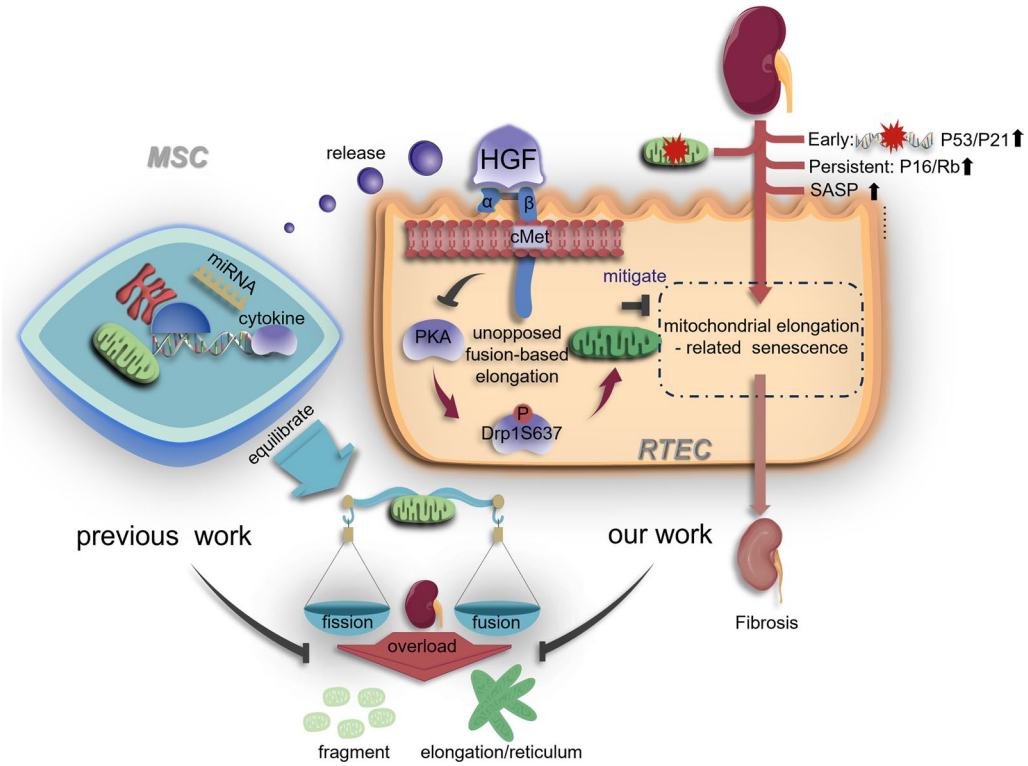

Fig. 10 Graphical abstract A model depicting the regulation of mitochondrial dynamics by hUC-MSCs-derived HGF during ischemia/reperfusion-induced senescence

Conclusion

Our work reveals a previously unrecognized role of hUC-MSCs-derived HGF in alleviating renal senescence and preventing progressive fibrosis in post-AKI through inhibiting mitochondrial elongation mediated by PKA-Drp1S637 signaling. Mitochondrial elongation control in stem cell-based therapy was first explored in kidney disease. We hope it will pave the way for renal senescence-targeted therapy and mitochondrial-targeted drug development.

Abbreviations

hUC-MSCs	human umbilical cord-derived mesenchymal stem cells
post-AKI	post-acute kidney injury
Col-MSCs	collagen matrix-encapsulated MSCs
uIRI	unilateral ischemia/reperfusion injury
HGF	hepatocyte growth factor
PKA	protein kinase A
Drp1pS637	inhibitory phosphorylation of drp1 at ser637 site
OMM	mitochondrial outer membrane

Supplementary Information

The online version contains supplementary material available at https://doi.org/10.1186/s13287-024-04041-3.

Additional file 1: Original unedited blot for Figure.

Additional file 2: ARRIVE checklist.

Acknowledgements

Not applicable.

Author contributions

KTZ conceived studies, designed experiments, interpreted results, and wrote the article. WJW and CX revised the article. XMZ, XRG, and XJR constructed the mouse model and did the immunohistochemistry. WJS prepared transmission electron microscope samples and captured images. QXH provide technical asistance. ZF and GYC provided experimental funds. XMC provided an experimental environment.

Funding

This work was supported by the Natural Science Foundation of China (82170686), the National Key Research and Development Program of China (2022YFC3602900), and the Grant for GYC (22KJLJ001).

Availability of data and materials

Not applicable.

Declarations

Ethics approval and consent to participate

hUC-MSCs used in this study were donated by Vcanbio Cell & Gene Engineering Corp. Ltd, which had confimmed that there was initial ethical approval for collection of human cells, and that informed consent was duly signed by the donors. The animal experiments were conducted in line with the ARRIVE guidelines 2.0. All animal experiments were performed under ethical supervision and approved by the Institutional Animal Care and Use Committee of the Chinese PLA General Hospital in 2022 (Title research: Study on stem cell therapy for acute kidney injury. No. 2022-X18-39). This ethics approval also permitted performing experiments using the aforementioned hUC-MSCs.

Consent for publication
Not applicable.

Competing interests
The authors declare that they have no competing interests.

Author details
[1]Medical School of Chinese PLA, Beijing 100853, China. [2]Department of Nephrology, First Medical Center of Chinese PLA General Hospital, National Key Laboratory of Kidney Diseases, Beijing Key Laboratory of Kidney Diseases Research, National Clinical Research Center for Kidney Diseases, Beijing 100853, China. [3]School of Medicine, Nankai University, Tianjin, China. [4]Department of Nephrology, Beijing Chao-Yang Hospital, Capital Medical University, Beijing, China.

Received: 29 March 2024 Accepted: 2 November 2024
Published online: 19 November 2024

References

1. Hoste EAJ, Kellum JA, Selby NM, et al. Global epidemiology and outcomes of acute kidney injury. Nat Rev Nephrol. 2018;14:607–25.
2. Chawla LS, Eggers PW, Star RA, et al. Acute kidney injury and chronic kidney disease as interconnected syndromes. N Engl J Med. 2014;371:58–66.
3. Li C, Shen Y, Huang L, et al. Senolytic therapy ameliorates renal fibrosis postacute kidney injury by alleviating renal senescence. FASEB J: Off Publ Fed Am Soc Exp Biol. 2021;35:e21229.
4. Li S, Livingston MJ, Ma Z, et al. Tubular cell senescence promotes maladaptive kidney repair and chronic kidney disease after cisplatin nephrotoxicity. JCI Insight. 2023. https://doi.org/10.1172/jci.insight.166643.
5. Huang W, Hickson LJ, Eirin A, et al. Cellular senescence: the good, the bad and the unknown. Nat Rev Nephrol. 2022;18:611–27.
6. Tang C, Cai J, Yin XM, et al. Mitochondrial quality control in kidney injury and repair. Nat Rev Nephrol. 2021;17:299–318.
7. Miwa S, Kashyap S, Chini E, et al. Mitochondrial dysfunction in cell senescence and aging. J Clin Investig. 2022. https://doi.org/10.1172/JCI158447.
8. Kim YY, Um JH, Yoon JH, et al. p53 regulates mitochondrial dynamics by inhibiting Drp1 translocation into mitochondria during cellular senescence. FASEB J Off Publ Fed Am Soc Exp Biol. 2020;34:2451–64.
9. Yoon YS, Yoon DS, Lim IK, et al. Formation of elongated giant mitochondria in DFO-induced cellular senescence: involvement of enhanced fusion process through modulation of Fis1. J Cell Physiol. 2006;209:468–80.
10. Wang WJ, Chen XM, Cai GY. Cellular senescence and the senescence-associated secretory phenotype: potential therapeutic targets for renal fibrosis. Exp Gerontol. 2021;151:111403.
11. Rodrigues CE, Capcha JM, de Bragança AC, et al. Human umbilical cord-derived mesenchymal stromal cells protect against premature renal senescence resulting from oxidative stress in rats with acute kidney injury. Stem Cell Res Ther. 2017;8:19.
12. Zhao L, Hu C, Zhang P, et al. Mesenchymal stem cell therapy targeting mitochondrial dysfunction in acute kidney injury. J Transl Med. 2019;17:142.
13. Perico L, Morigi M, Rota C, et al. Human mesenchymal stromal cells transplanted into mice stimulate renal tubular cells and enhance mitochondrial function. Nat Commun. 2017;8:983.
14. Jia Y, Cao N, Zhai J, et al. HGF mediates clinical-grade human umbilical cord-derived mesenchymal stem cells improved functional recovery in a senescence-accelerated mouse model of Alzheimer's disease. Adv Sci. 2020;7:1903809.
15. Piao L, Huang Z, Inoue A, et al. Human umbilical cord-derived mesenchymal stromal cells ameliorate aging-associated skeletal muscle atrophy and dysfunction by modulating apoptosis and mitochondrial damage in SAMP10 mice. Stem Cell Res Ther. 2022;13:226.
16. Huang M, Li D, Chen J, et al. Comparison of the treatment efficacy of umbilical mesenchymal stem cell transplantation via renal subcapsular and parenchymal routes in AKI-CKD mice. Stem Cell Res Ther. 2022;13:128.
17. Wang B, Li ZL, Zhang YL, et al. Hypoxia and chronic kidney disease. EBioMedicine. 2022;77:103942.
18. Liu M, Wang W, Wang J, et al. Z-Guggulsterone alleviates renal fibrosis by mitigating G2/M cycle arrest through Klotho/p53 signaling. Chem Biol Interact. 2022;354:109846.
19. Ko HJ, Tsai CY, Chiou SJ, et al. The phosphorylation status of Drp1-Ser637 by PKA in mitochondrial fission modulates mitophagy via PINK1/Parkin to exert multipolar spindles assembly during Mitosis. Biomolecules. 2021. https://doi.org/10.3390/biom11030424.
20. Lee D-S, Kim T-H, Park H, et al. CDDO-me attenuates clasmatodendrosis in CA1 astrocyte by inhibiting HSP25-AKT mediated DRP1-S637 phosphorylation in chronic epilepsy rats. Int J Mol Sci. 2022. https://doi.org/10.3390/ijms23094569.
21. Loh J-K, Lin C-C, Yang M-C, et al. GSKIP- and GSK3-mediated anchoring strengthens cAMP/PKA/Drp1 axis signaling in the regulation of mitochondrial elongation. Biochim Biophys Acta. 2015;1853:1796–807.
22. Boichuck M, Zorea J, Elkabets M, et al. c-Met as a new marker of cellular senescence. Aging. 2019;11:2889–97.
23. Ferenbach DA, Bonventre JV. Mechanisms of maladaptive repair after AKI leading to accelerated kidney ageing and CKD. Nat Rev Nephrol. 2015;11:264–76.
24. Docherty MH, O'Sullivan ED, Bonventre JV, et al. Cellular senescence in the kidney. J Am Soc Nephrol. 2019;30:726–36.
25. Zhang JQ, Li YY, Zhang XY, et al. Cellular senescence of renal tubular epithelial cells in renal fibrosis. Front Endocrinol. 2023;14:1085605.
26. Horbay R, Bilyy R. Mitochondrial dynamics during cell cycling. Apoptosis Int J Program cell death. 2016;21:1327–35.
27. Li D, Li X, Guan Y, et al. Mitofusin-2-mediated tethering of mitochondria and endoplasmic reticulum promotes cell cycle arrest of vascular smooth muscle cells in G0/G1 phase. Acta Biochim Biophys Sin. 2015;47:441–50.
28. Yamada T, Adachi Y, Fukaya M, et al. Dynamin-related protein 1 deficiency leads to receptor-interacting protein kinase 3-mediated necroptotic neurodegeneration. Am J Pathol. 2016;186:2798–802.
29. Gomes LC, Di Benedetto G, Scorrano L. During autophagy mitochondria elongate, are spared from degradation and sustain cell viability. Nat Cell Biol. 2011;13:589–98.
30. Dai L, Trillo-Tinoco J, Cao Y, et al. Targeting HGF/c-MET induces cell cycle arrest, DNA damage, and apoptosis for primary effusion lymphoma. Blood. 2015;126:2821–31.
31. Martini H, Passos JF. Cellular senescence: all roads lead to mitochondria. FEBS J. 2023;290:1186–202.
32. Bugarski M, Ghazi S, Polesel M, et al. Changes in NAD and lipid metabolism drive acidosis-induced acute kidney injury. J Am Soc Nephrol. 2021;32:342–56.
33. Phadwal K, Tang QY, Luijten I, et al. p53 regulates mitochondrial dynamics in vascular smooth muscle cell calcification. Int J Mol Sci. 2023. https://doi.org/10.3390/ijms24021643.
34. Chou CH, Lin CC, Yang MC, et al. GSK3beta-mediated Drp1 phosphorylation induced elongated mitochondrial morphology against oxidative stress. PLoS ONE. 2012;7:e49112.
35. Merrill RA, Dagda RK, Dickey AS, et al. Mechanism of neuroprotective mitochondrial remodeling by PKA/AKAP1. PLoS Biol. 2011;9:e1000612.
36. Li S, Lin Q, Shao X, et al. Drp1-regulated PARK2-dependent mitophagy protects against renal fibrosis in unilateral ureteral obstruction. Free Radical Biol Med. 2020;152:632–49.
37. Wang Y, Lu M, Xiong L, et al. Drp1-mediated mitochondrial fission promotes renal fibroblast activation and fibrogenesis. Cell Death Dis. 2020;11:29.
38. Youle RJ, van der Bliek AM. Mitochondrial fission, fusion, and stress. Science. 2012;337:1062–5.
39. Kim Y-M, Youn S-W, Sudhahar V, et al. Redox regulation of mitochondrial fission protein Drp1 by protein disulfide isomerase limits endothelial senescence. Cell Rep. 2018;23:3565–78.
40. You Y, Chen X, Chen Y, et al. Epigenetic modulation of Drp1-mediated mitochondrial fission by inhibition of S-adenosylhomocysteine hydrolase promotes vascular senescence and atherosclerosis. Redox Biol. 2023;65:102828.
41. Xu L, Wang J, Yu H, et al. GLIS1 alleviates cell senescence and renal fibrosis through PGC1-α mediated mitochondrial quality control in kidney aging. Free Radical Biol Med. 2023;209:171–84.

42. Wang H-H, Wu Y-J, Tseng Y-M, et al. Mitochondrial fission protein 1 up-regulation ameliorates senescence-related endothelial dysfunction of human endothelial progenitor cells. Angiogenesis. 2019;22:569–82.
43. Archer SL. Mitochondrial dynamics–mitochondrial fission and fusion in human diseases. N Engl J Med. 2013;369:2236–51.
44. Losón OC, Song Z, Chen H, et al. Fis1, Mff, MiD49, and MiD51 mediate Drp1 recruitment in mitochondrial fission. Mol Biol Cell. 2013;24:659–67.

Publisher's Note